Experimental Investigation of Nonlinear Cyclic Behavior of Circular Concrete Bridge Piers with Pitting Corrosion

Mohammad M. Kashani[1]; Hamish Moodley[2]; Hammed O. Aminulai[3]; Sheida Afshan[4]; and Duncan Crump[5]

Abstract: In this study, three reinforced concrete (RC) columns with and without corrosion and different reinforcement details are tested under lateral cyclic loading. One of these columns is well-confined to represent modern RC bridge piers that are designed according to the current seismic design codes, and the second column has the same detail with corrosion damage. The third column is a lightly confined corroded column to represent aging RC bridge piers that are not designed to the current seismic design codes. The experimental results showed that corrosion significantly impacts the ductility loss more than the strength loss of the tested corroded columns. In addition, although the uncorroded column was designed according to the current seismic design code, severe inelastic buckling in the vertical bars was observed during the cyclic tests. **DOI: 10.1061/JBENF2.BEENG-6482**. © *2024 American Society of Civil Engineers*.

Author keywords: Bridge pier; Corrosion; Inelastic buckling; Nonlinear behavior; Reinforced concrete; Seismic performance.

Introduction

Many transport infrastructures worldwide are subject to material aging. The deterioration of concrete bridges, the most critical nodes in any transport infrastructure network, is recognized as one of the major challenges faced by the bridge engineering community. Reinforced concrete (RC) structures are vulnerable to deterioration effects that are caused by chloride-induced corrosion (from deicing salts and seawater) and, to a lesser extent, by carbonation (GCM, Gaal 2004). Chloride-induced corrosion of reinforcing steel is the most significant environmental threat that affects the performance of aging RC bridges and structures in the UK and worldwide (Broomfield 2023). Severe corrosion and insufficient reinforcement detail have resulted in several catastrophic failures worldwide (e.g., the Monardi Bridge collapse in Italy, the De la Concorde Bridge collapse in Canada, and the Ynys-y-Gwas Bridge collapse in the UK), or severe disruption in traffic flow due to the bridge closure (e.g., Hammersmith Flyover in London, which carried 100,000 vehicles per day). England's strategic and local road networks have a net worth of £344 billion (Barker et al. 2014). Corrosion damage to RC bridges is estimated to cost approximately £1 billion/year in England and Wales (Barker et al. 2014), which represents approximately 10% of the total UK bridge inventory. The estimated direct cost to repair aging infrastructure in the US is over $200 billion (Angst 2018; ASCE 2021).

A large portion of aging corroded RC bridges are in high seismicity regions. Therefore, several researchers (Biondini et al. 2015; Camnasio 2013; Dizaj et al. 2018a, b 2023; Ghosh and Padgett 2010; Li et al. 2015; Rao et al. 2017) have investigated the impact of corrosion on the seismic fragility and life cycle cost of RC structures using simplified models. The focus of these studies was on numerical modeling and probabilistic studies on the effect of corrosion on the seismic fragility of aging bridges. They concluded that the deterioration in bridges due to reinforcement corrosion has a significant negative influence on the structural vulnerability of RC bridges and significantly increases the life cycle cost of these bridges. Other researchers (Du et al. 2005a; Di Carlo et al. 2023; Du et al. 2005b; Imperatore et al. 2017; Lee and Cho 2009; Kashani 2017; Kashani et al. 2015a, b; Kashani et al. 2013) investigated the impact of corrosion on the residual capacity of reinforcing bars that were subject to monotonic tension and compression and cyclic loading that included the effects of inelastic buckling and low-cycle fatigue. The outcomes of these studies provided a modeling approach to simulate the uniaxial material behavior of corroded bars under different loading scenarios. Limited experimental studies have been conducted to investigate the impact of corrosion on the nonlinear behavior of RC components (Ge et al. 2020; Lee et al. 2003; Liu et al. 2017; Meda et al. 2014; Rajput and Sharma 2018; Rinaldi et al. 2022; Yuan et al. 2017; Yang et al. 2016). The focus of these studies was on corroded RC beams or rectangular or square RC columns. The outcomes of previous experimental observations confirmed that corrosion has a significant negative impact on residual strength, multiple failure modes (e.g., flexure or shear–flexure failure), and the overall ductility of RC components (Ge et al. 2020; Lee et al. 2003; Liu et al. 2017; Meda et al. 2014; Rajput and Sharma 2018; Rinaldi et al. 2022; Yuan et al. 2017; Yang et al. 2016).

Kashani et al. (2019) report the results of a literature survey on the available experimental data of corroded RC components. Their results revealed that most of the previous research on the

[1]Associate Professor, Univ. of Southampton Boldrewood Innovation Campus, Burgess Rd., Room 4019, Building 178, Southampton SO16 7QF, UK. ORCID: https://orcid.org/0000-0003-0008-0007. Email: mehdi.kashani@soton.ac.uk

[2]Ph. D. Candidate, Univ. of Southampton Boldrewood Innovation Campus, Burgess Rd., Building 178, Southampton SO16 7QF, UK (corresponding author). ORCID: https://orcid.org/0009-0008-3808-3696. Email: h.t.m.moodley@soton.ac.uk

[3]Ph. D. Candidate, Univ. of Southampton Boldrewood Innovation Campus, Burgess Rd., Building 178, Southampton SO16 7QF, UK. ORCID: https://orcid.org/0000-0001-6185-5000. Email: h.o.aminulai@soton.ac.uk

[4]Associate Professor, Univ. of Southampton Boldrewood Innovation Campus, Burgess Rd., Room 4021, Building 178, Southampton SO16 7QF, UK. Email: s.afshan@soton.ac.uk

[5]Experimental Officer, Large-Scale Structural Testing Laboratory (LSTL), Univ. of Southampton, Boldrewood Innovation Campus, Building 178, Burgess Rd., Southampton SO16 7QF, UK. ORCID: https://orcid.org/0000-0002-6409-040X. Email: d.a.crump@soton.ac.uk

Note. This manuscript was submitted on May 31, 2023; approved on January 6, 2024; published online on May 17, 2024. Discussion period open until October 17, 2024; separate discussions must be submitted for individual papers. This paper is part of the ***Journal of Bridge Engineering***, © ASCE, ISSN 1084-0702.

experimental testing of corroded RC structural components had been focused on beams under monotonic and cyclic loading (flexure and shear) and rectangular or square columns that were subject to lateral cyclic loading. Limited reliable experimental data is currently available in the literature to investigate the nonlinear cyclic behavior of circular corroded RC columns (Aquino and Hawkins 2007; Ma et al. 2012; Yuan et al. 2017). Circular columns are very common in bridge pier construction, and their failure mechanism is very different from that of rectangular or square columns due to the difference in their geometry. Therefore, experimental investigations of the nonlinear behavior of corroded circular columns subject to cyclic loading are required.

Research Novelty and Contribution

As discussed in the previous section of this study, there is a significant lack of reliable experimental data in the literature on nonlinear cyclic behavior and seismic performance of circular corroded RC bridge piers. Most aging circular corroded bridge piers were designed and constructed before the modern seismic design codes (pre-1990s). The recently constructed circular RC bridges, which are designed and built according to modern seismic codes, are vulnerable to corrosion. Therefore, the nonlinear behavior of the new and old generations of corroded circular bridge piers that are subject to lateral cyclic loading must be investigated. Currently, no experimental data exists in the literature to investigate and compare the impact of corrosion on code-conforming and non-code-conforming circular RC columns to the best of the authors' knowledge. Therefore, this experimental study aims to address this gap by conducting benchmark experimental tests on circular corroded RC columns with different reinforcement details. The test specimens consist of corroded and uncorroded columns, which are designed according to Eurocode 2 (CEN 2004) and are seismically detailed according to Eurocode 8 (EC8; CEN 2005) to represent a new bridge design. A further corroded column is designed to have the same flexural capacity as the other two columns but without seismic reinforcement, with details to represent old or non-code-conforming bridge piers (premodern seismic design codes). The only difference between the two groups of columns is the volumetric ratio of the confinement reinforcement, which is the most important parameter in the nonlinear seismic behavior of RC bridge piers. The experimental results showed that pitting corrosion significantly impacts the ductility and hysteretic energy dissipation capacity of RC columns and, to a lesser extent, their residual strengths.

Experimental Program

Specimen Design and Properties

Three circular RC columns 400 mm diameter cross section and 1,600 mm high (height above the foundation) were designed according to Eurocode 2 (CEN 2004). The column section contained nine 16 mm diameter vertical bars. Two columns were detailed for seismic loading according to EC8 (CEN 2005), with the tie reinforcement spaced at 80 mm. The third column was designed according to Eurocode 2 (CEN 2004) with the same flexural capacity as the other two columns, but it was not detailed for seismic loading, with the tie reinforcement spaced at 200 mm. This column represented the non-code-conforming old bridge design with light confining reinforcement. The cover concrete was 30 mm, and the maximum aggregate size of the concrete was 10 mm. Fig. 1 shows the details of the column specimens, and Table 1 lists the experimental test matrix and associated concrete strength. Tables 2 and 3 summarize the mechanical properties of the steel and concrete mix that was used in test specimens, and Fig. 2 shows the nonlinear stress–strain behavior of the 8 and 16 mm diameter bars.

Accelerated Corrosion Procedure

The natural corrosion in RC structures on-site is a gradual process that takes several years. Researchers have employed various corrosion simulation methods in laboratory settings to accelerate the deterioration in RC test specimens. Previous studies have utilized techniques such as the external current method (El Maaddawy and Soudki 2003), preadmixed chlorides (El Maaddawy and Soudki 2003), and cyclic wetting and drying (Otieno et al. 2019) to expedite corrosion. In this study, an accelerated corrosion procedure was adopted that has been successfully employed in previous research that was conducted by the authors (Aminulai et al. 2023a, b; Ge et al. 2020).

The detailed methodology for this accelerated corrosion procedure, which uses external current methods and the corresponding experimental setup, can be found in the literature (Aminulai et al. 2023a, b; Ge et al. 2020). In brief, the approach involved establishing an electrochemical circuit that used an external power source. Within this setup, the reinforcing bars function as the anode, and an external material serves as the cathode. Common cathode materials include copper, stainless steel, and regular carbon steel. An electrolyte, typically a saline solution, facilitates the flow of ionic current from the embedded reinforcement to the external cathode. This experiment used stainless steel plates as the external cathode, paired with a 5% sodium chloride (NaCl) saline solution.

The accelerated corrosion procedure took 8 and 6 weeks for Columns A1 and B1, respectively. During this period, the average current applied was 5 A. Fig. 3 shows the corroded columns after the accelerated corrosion procedure, where some surface horizontal and vertical cracks were observed. The vertical cracks were due to the corrosion of the longitudinal or vertical reinforcing bars, and the horizontal cracks were due to the corrosion of horizontal hoop or tie reinforcements.

Reaction Frame Test Setup, Instrumentation, and Loading Protocol

A specially designed test rig for performing lateral cyclic loading on large-scale structural components was utilized for the column tests in the Large Structures Testing Laboratory (LSTL) at the University of Southampton, UK. Fig. 4 shows the adopted test setup, which involved a 250 kN capacity MTS Systems Corporation (Eden Prairie, MA) actuator with a 250 mm stroke to apply the lateral cyclic loading. The columns were not subjected to axial loads. The reaction frame and the foundation block were fixed to the laboratory's strong floor using pretensioned steel rods to prevent movement during testing. Lateral displacement was applied at 1.8 m at the top of the column using a displacement-controlled loading scheme, as shown in Fig. 5. The lateral displacements were from 1.6 to 96 mm, with two repeated cycles for each lateral deformation level, as recommended by ACI 374.2R-13 (ACI 2013). Lateral displacement in the direction away from and toward the reaction frame was assigned as positive and negative, respectively.

The measurement instrumentation utilized in the tests was composed of five 5 linear variable differential transformer to measure the displacement in the column at different heights and digital image correlation (DIC) to capture the full-field strain in the plastic hinge region of the columns. DIC is a noncontact imaging technique that measures displacements and strains in structures as they deform. The process involves taking a reference image of the region of

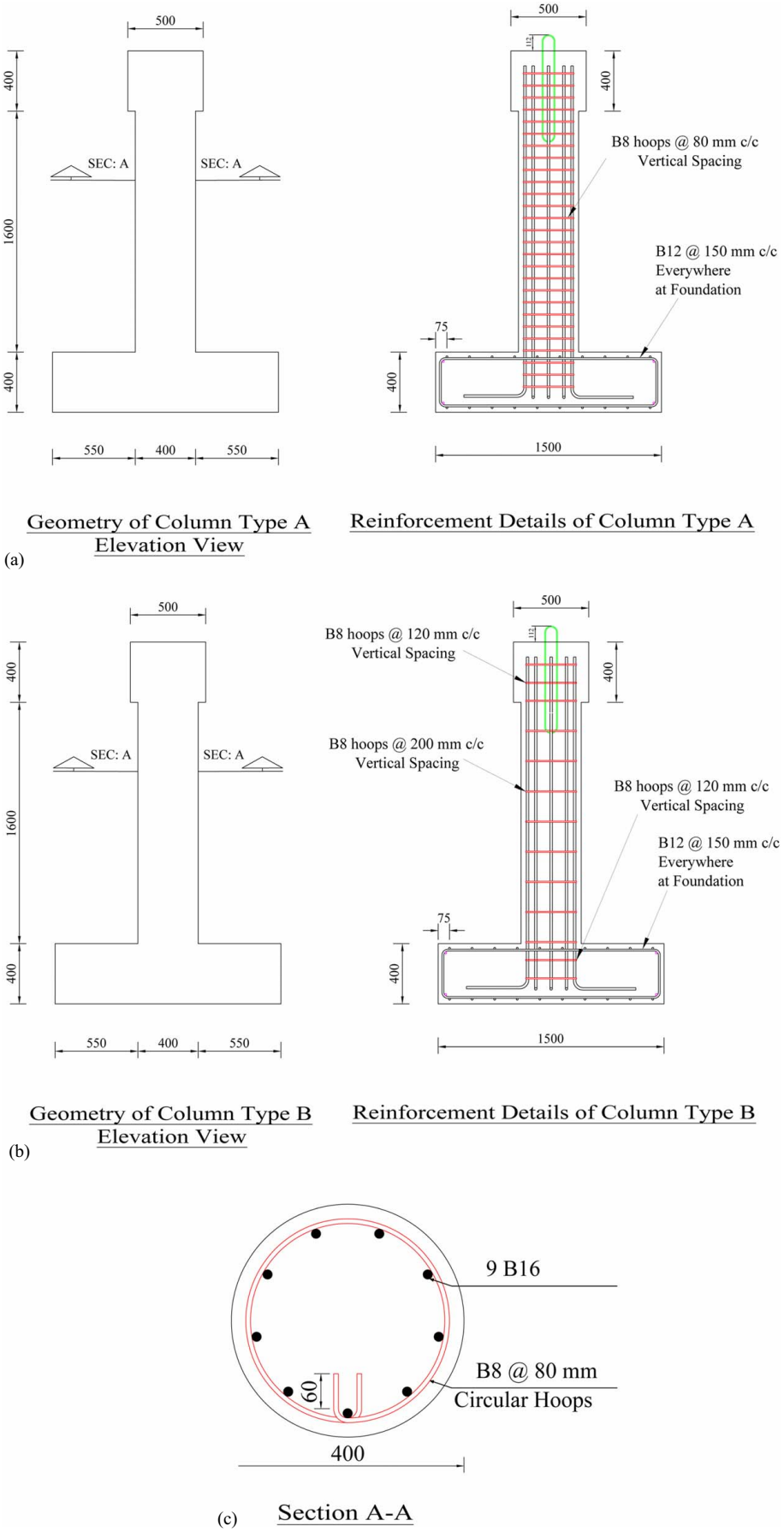

Fig. 1. Experimental test specimens: (a) dimensions and reinforcement details of Column A; (b) dimensions and reinforcement details of Column B; and (c) cross section of Columns A and B (mm).

Table 1. Experimental test matrix

Column ID	Design	28 days cube mean strength	Estimated mass loss
Column A	Well-confined	75.4 MPa	0
Column A1	Well-confined	73.7 MPa	20%
Column B1	Lightly confined	62.6 MPa	20%

Table 2. Mechanical properties of uncorroded steel reinforcement

Reinforcement type	8 mm (B8)	16 mm (B16)
Yield strength [f_y (MPa)]	520	530
Modulus of elasticity [E_s (MPa)]	200,426	193,913
Yield strain (ε_y)	0.00261	0.00273
Ultimate tensile strength [f_u (MPa)]	645	640
Strain at ultimate tensile strength (ε_u)	0.057	0.165
Fracture strain (ε_f)	0.152	0.227
Unit mass [m (kg/m)]	0.396	1.579

Table 3. Concrete mix in 1 m^3 (water/cement ratio = 0.39)

Mix constituent	Quantity
Cement (52R)	420 kg
4–10 mm stone (flint)	901 kg
0–4 mm sand	823 kg
Superplasticizer	1.8 L
Total water	160 kg

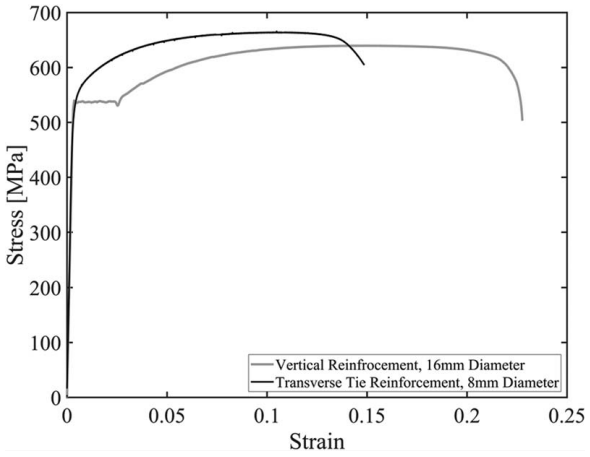

Fig. 2. Stress–strain behavior of vertical and horizontal tie reinforcement.

interest on the column specimen before deformation occurs, followed by continuously capturing images during deformation (the deformed images). Then, the deformed images are compared with the reference image to compute displacements and strains in the region of interest. A random speckle pattern is applied to the specimen to enable image comparison. These speckles are grouped in DIC into subsets of at least three speckles. The deformation in each subset is used to correlate the displacements and strains in the plastic hinge region of the column. Because the column was circular with a curved surface, stereo DIC with multiple cameras was employed. For these tests, four Manta G504-B cameras, Stadtroda, Germany with two Nikon, Tokyo, Japan AF 50 mm f/1.8D lenses and two Nikon 28 mm f/2.8D lenses were used to film at a frame rate of 1 Hz during testing. The DIC images were processed using MatchID Stereo software, Gent, Belgium. Fig. 6 shows an example of a DIC speckle pattern. In addition, the cameras, settings and parameters that were used in the DIC are presented in Table 4.

Corrosion Measurement

After structural tests, the corroded columns were carefully demolished, and the mass loss of each vertical bar and hoop reinforcement was measured. The demolished columns were divided into three segments along their height. For each segment, the corrosion in all individual bars and hoop reinforcement was measured. The detailed mass loss calculation data are available in an Excel spreadsheet, which is attached to this paper. Table 5 lists the average measured corrosion for each segment, where the length of each segment was measured from the base. The corroded reinforcement for corroded Columns A1 and B1 is shown in Figs. 7 and 8. The bar labels relate to the detailed corrosion calculations in the attached data file.

Transfer Function Estimate of the Corroded Columns

One of the most popular methods to describe the frequency content of a time series is power spectral density (PSD) (Chan and Cryer 2008). The PSD estimates could be used in system identification for structural health monitoring. The periodic pattern (if there is one) of a time series could be quantified by PSD by calculating the peaks in frequency which correspond to these periodicities. If the excitation and response of a linear system are known, a system identification could be performed by estimating the transfer function (Chan and Cryer 2008). This system identification method could be used in corroded columns before and after corrosion to identify the impact of corrosion on the effective stiffness and dynamic properties of column specimens.

In this study, the impact hammer tests (Liu et al., 2022) is used to estimate the transfer function. Each column was instrumented with two accelerometers in the longitudinal and transverse directions. Five impact tests in each direction were performed and the average transfer function was estimated (Verboven et al. 2005) for each direction. Fig. 8 shows the transfer function estimates for Columns A1 and B1 before and after corrosion.

The frequency that is associated with the first peak in the transfer function is the frequency of the first mode of vibration (i.e., the natural frequency of the system). Fig. 9 shows that corrosion increased the natural frequency of both columns. Fig. 9(a) shows that the natural frequency of Column A1 was 8.5 Hz before corrosion and 9.5 Hz after corrosion. Fig. 9(b) shows that the natural frequency of Column B1 was 12 Hz before corrosion and 14.5 Hz after corrosion. This showed that although corrosion resulted in damage to concrete, the internal volumetric pressure due to the expansion of rust products could increase the stiffness of the column. This is important when estimating the initial effective stiffness of columns for seismic assessments and evaluating corroded columns. The impact of corrosion on the stiffness degradation during the cyclic loading experiments is discussed in the relevant section "Impact of Corrosion on Effective Stiffness Degradation of RC Columns."

Experimental Test Results and Discussion

Nonlinear Cyclic Response of Well-Confined Uncorroded Column A

Fig. 10 shows the nonlinear cyclic response of the uncorroded Column A with the failure points that correspond to the first and second fractures in the vertical reinforcement bars marked. The key damage states are shown in Fig. 11. The flexural cracks due to reinforcement yielding started appearing at approximately 5% drift. At approximately 2% drift, the column base to foundation

Fig. 3. Corroded columns: (a) Column A1; and (b) Column B1.

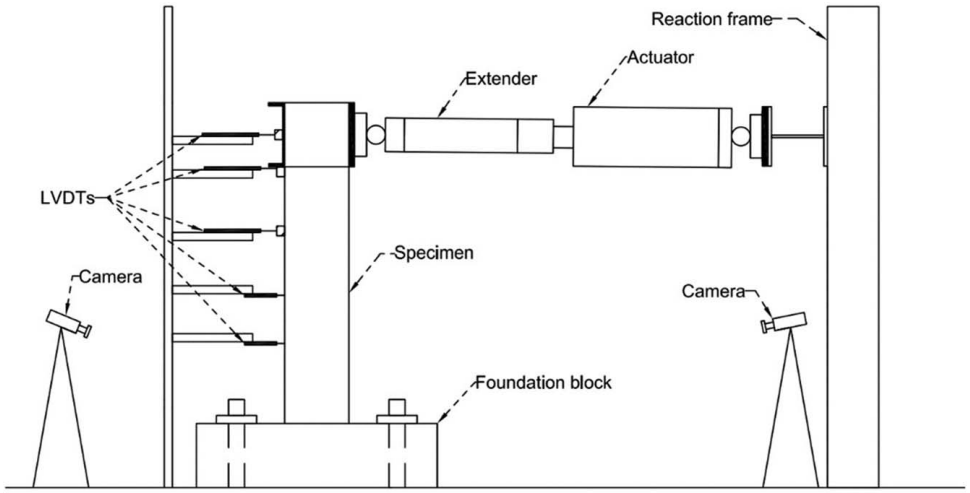

Fig. 4. Experimental test setup.

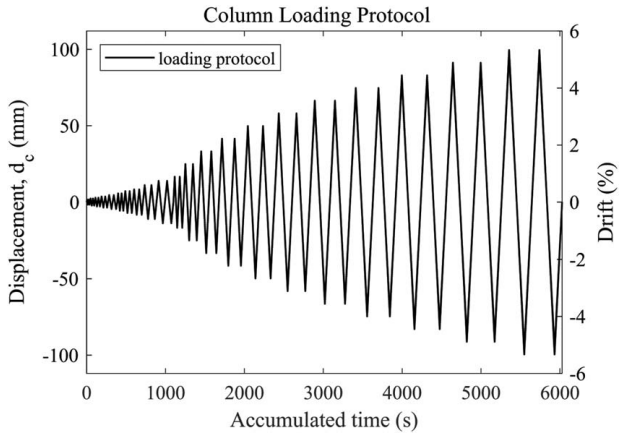

Fig. 5. Loading protocol.

connection started splitting, which was a sign of reinforcement slip and strain penetration at the column base [Fig. 11(a)]. As the loading amplitude increased, at approximately 3% drift, the concrete cover started to crush at the front face of the column [Fig. 11(b)]. At 4% drift, significant visible buckling in the vertical reinforcing bars at the front face of the column was observed [Fig. 11(c)]. Because the concrete cover crushing started at 3% from the face, this confirmed that bar buckling started at a lower drift, which resulted in concrete cover spalling. Following the severe bar buckling, the first buckled bar fractured in the next cycle at 4.5% drift [Fig. 11(d)]. Finally, in the final cyclic amplitude targeted at 5.5% drift, the second buckled bar fractured at 4.5% during reloading from compression to tension [Fig. 11(e)]. The failure mechanism in the buckled bars confirmed that both bars fractured during the unloading phase when they were still in compression. This was due to the combination of significant inelastic buckling and low-cycle fatigue in the vertical bars, which agreed well with

Fig. 6. Speckle pattern for DIC.

the findings reported by other researchers (Meda et al. 2014; Ge et al. 2020). In EC8 (CEN 2005), hoop spacing ($S_L \leq 6$) times the longitudinal bar diameter (d_b) is suggested. In this study, the S_L/d_b ratio was five, but buckling of the vertical bars and yielding of hoop reinforcement were observed. The experimental results show that the interaction between the stiffness of the hoop reinforcement and the flexural rigidity of the vertical bars is an important factor in the seismic detailing of RC columns, which supports the findings reported by other researchers (Dhakal and Maekawa 2002). This is not explicitly captured in the current code, which is an area for further research.

Nonlinear Cyclic Response of Well-Confined Corroded Column A1

Fig. 12 shows the nonlinear cyclic response of corroded Column A1. The identified failure points are shown in Fig. 12, and the corresponding damage is shown in Fig. 13. The corrosion was localized at the bottom of the column; therefore, the column foundation interface's vertical bar slippage and delamination occurred at approximately 2% drift [Fig. 13(a)] similar to Column A [Fig. 11(a)]. However, in Column A1, Most of the column deformation was concentrated at the base of the column, and therefore, limited flexural cracks were observed during the cyclic tests. As the drift ratio increased, the concrete cover spalled at approximately 3% drift [Fig. 13(b)], followed by a fracture in the first and the second vertical bars at 3.5% drift [Fig. 13(c)]). Finally, the third vertical bar fractured at approximately 4% drift [Fig. 13(d)], which resulted in a complete failure of the column. This failure mode differed completely from the failure mode in the same column without corrosion. This was due to the localized corrosion of a few vertical reinforcement bars at the base of the column. Table 3 indicates that

Table 4. Cameras, settings, and parameters used in stereo DIC

Cameras, settings, and parameters	Negative loading direction side	Positive loading direction side
Sensor and digitization	CCD 2,456 × 2,058 pixels, 8-bit	CCD 2,456 × 2,058 pixels, 8-bit
Exposure time and recording rate	190,00 μs, 1 Hz	19,000 μs, 1 Hz
Mean camera noise (% of dynamic range)	0.0037%; 0.0034%	0.0033%; 0.0034%
Lens and imaging distance	Nikkor 50 mm, 2.69 m	Nikkor 28 mm, 1.55 m
Number of images averaged for resolution calculation	2	2
Pixel size	3.45 μm	3.45 μm
Region of interest and field of view	100 × 200 mm, 442 × 370 mm	100 × 200 mm, 537 × 450 mm
Subset, step	59, 16 pixels	59, 16 pixels
Matching criterion Interpolation, shape function	ZNSSD, Local Bicubic Spline, Quadratic	ZNSSD, Local Bicubic Spline, Quadratic
Presmoothing	None	None
Mean displacement resolution	0.0470 mm (1.45 pixels)	0.0586 mm (1.22 pixels)
Smoothing technique	None	None
Virtual strain gauge	7 pixels (24.15 μm)	7 pixels (24.15 μm)
Mean strain resolution	471 με	366 με

Note: CCD = Charge-coupled device.

Table 5. Measured mass loss in corroded columns

	Percentage mass loss in the reinforcement (%)					
	Longitudinal bars			Transverse ties		
Test specimen	Segment A[a]	Segment B[a]	Segment C[a]	Segment A[a]	Segment B[a]	Segment C[a]
Column A1	10.40%	5.32%	4.04%	21.78%	19.75%	17.18%
Column B1	12.98%	16.31%	12.68%	28.30%	39.63%	26.27%

[a]Segment A (0–200 mm); Segment B (200–400 mm); and Segment C (400–600 mm).

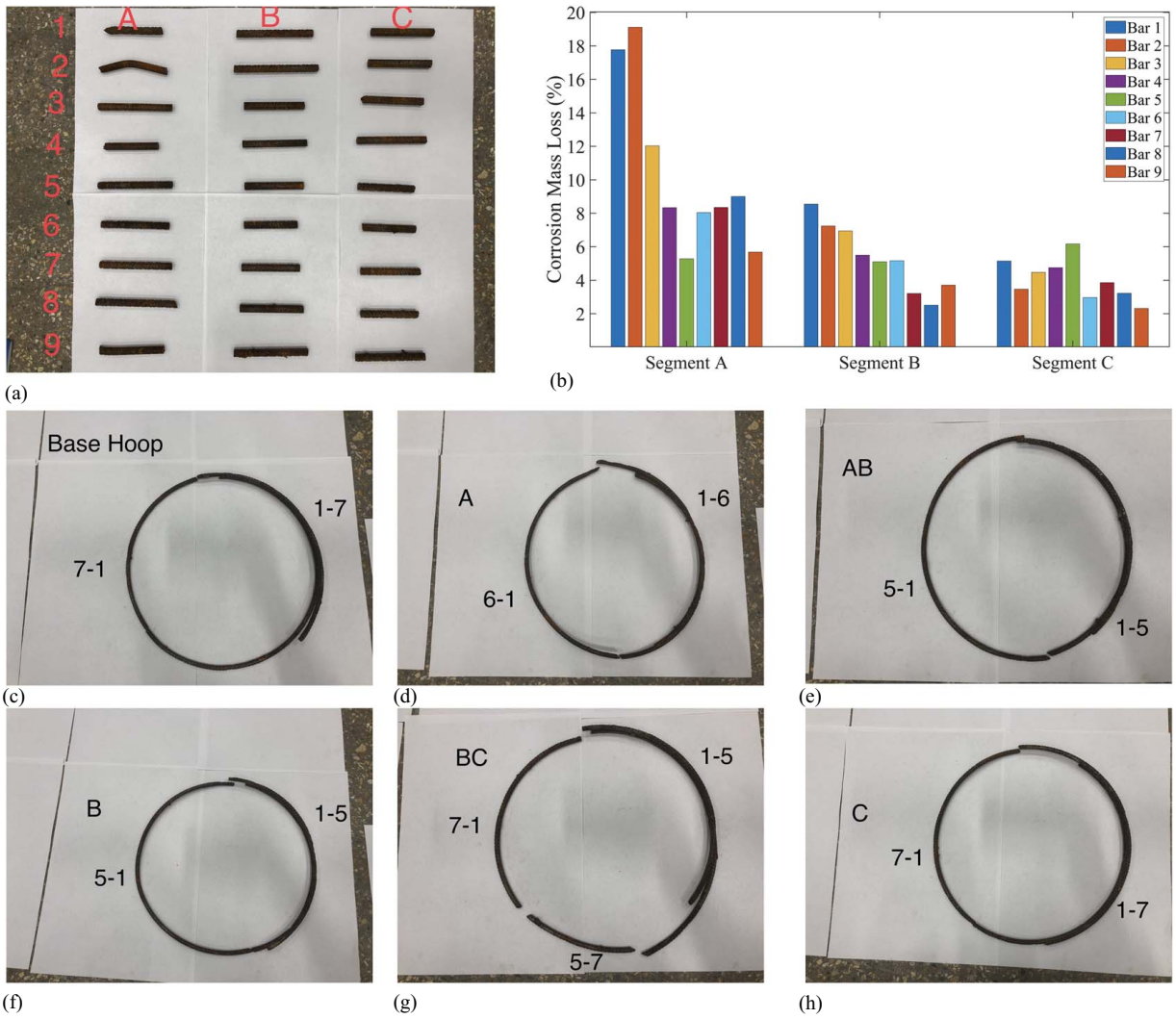

Fig. 7. Measured corrosion in Column A1 after cyclic test: (a) vertical bars in each segment; (b) mass loss of individual vertical bars; (c) and (d) hoop reinforcement in Segment A; (e) and (f) hoop reinforcement in Segment B; and (g) and (h) hoop reinforcement in Segment C.

the average corrosion of vertical bars within 200 mm above the foundation was 10.40%. However, the corrosion in Bars A1, A2, and A3 (these references are defined in the attached Excel file with detailed mass loss calculations) was 17.77%, 19.11%, and 12.03%, respectively, which was localized at the base of the column. This resulted in premature fracture in these bars at the base of the column.

Nonlinear Cyclic Response of Lightly Confined Corroded Column B1

Fig. 14 shows the nonlinear cyclic response of the corroded Column B1. The failure points are shown in Fig. 14, and the corresponding damage is in Fig. 15. The first visible flexural cracks started to appear at approximately 0.5% drift with a vertical crack along a corroded bar. The vertical crack was due to the corrosion crack that existed in the column, and its width increased during the test. At approximately 0.8% drift, premature spalling of the concrete cover on the back face of the column was observed [Fig. 15(a)]. This was approximately 400 mm above the foundation, where the concrete cover was partially spalled due to corrosion before the cyclic test. At approximately 2% drift, the first vertical bar fractured due to severe pitting corrosion followed by concrete cover spalling [Fig. 15(b)] during the load reversal from tension to compression. Visible bar buckling was observed at 3% drift [Fig. 15(c)], which was followed by core concrete crushing in the following cycle at 3.5% drift. At 4% drift, a corroded hoop fractured, which resulted in core concrete crushing. The significant localized or pitting corrosion 400 mm above the foundation was where the first vertical bar fractured. Here, corrosion resulted in a complete loss of the hoop reinforcement, which resulted in premature concrete cover spalling.

Digital Image Correlation

DIC could be employed to measure the crack damage and strain field on the surface of RC columns. Currently, a limited number of studies have utilized the method on curved surfaces (Al-Kamaki 2021; Sun et al. 2023). The processed DIC images show von Mises equivalent strain contour plots at the cracking moment, 1% drift, and drift at the ultimate strength of Columns A, A1, and B1 are shown in Fig. 16. For Column A, the DIC data show that flexural cracks occurred after the first lateral drift cycles (0.1% drift) [Fig. 16(a)], beyond which the number and strain in the flexural cracks increased at 1% drift [Fig. 16(b)] and at drift at ultimate strength [Fig. 16(c)]. The corroded Column A1 demonstrated a

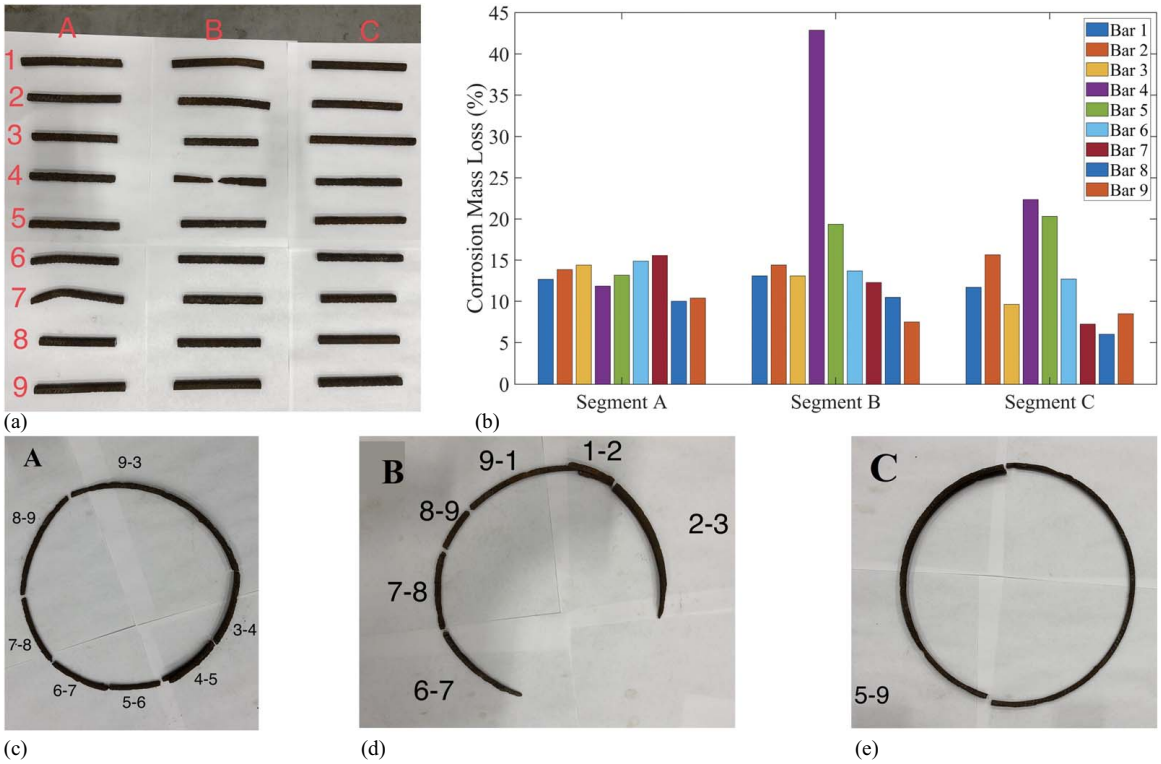

Fig. 8. Measured corrosion of Column B1 after cyclic test: (a) vertical bars in each Segment; (b) mass loss of individual vertical bars; (c) hoop reinforcement in Segment A; (d) hoop reinforcement in Segment B; and (e) hoop reinforcement in Segment C.

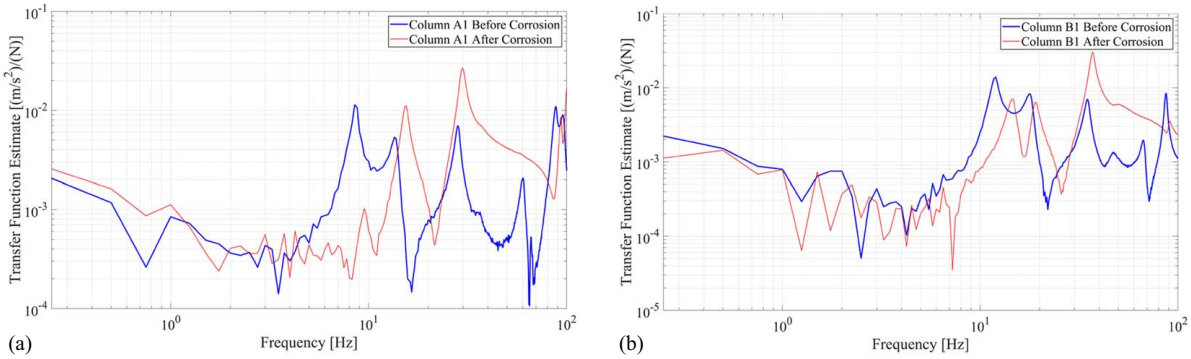

Fig. 9. Average transfer function estimates of (a) Column A1; and (b) Column B1.

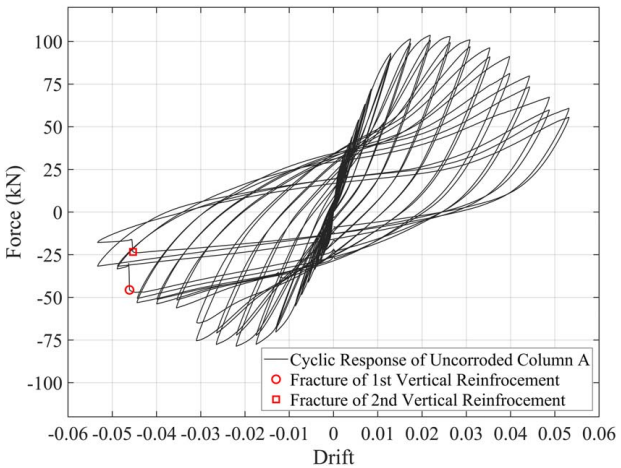

Fig. 10. Nonlinear cyclic response of uncorroded Column A.

similar crack development pattern as Column A. In addition to flexural cracks, Column A1 presented a vertical crack, which propagated downward as the lateral drift increased [Figs. 16(d–f)]. Column B1 demonstrated a lower number of flexural cracks during testing [Figs. 16(g–i)], due to the reduced confinement of this column and similar to Column A1, a singular vertical crack. These vertical cracks were above the corroded longitudinal reinforcement and occurred from the corrosion process. From the DIC strain plots [Figs. 16(a, d, and g)], the cracking in the concrete cover occurred at much lower drift values than the first visibly observed cracks.

The DIC images were utilized to obtain the strain in the vertical plane of the plastic hinge region from both loading sides of the columns. Then, the vertical strains from the extreme fibers in the columns in both loading directions were computed together. Euler–Bernoulli beam theory was assumed to obtain the position of the neutral axis, the strains on the longitudinal reinforcement,

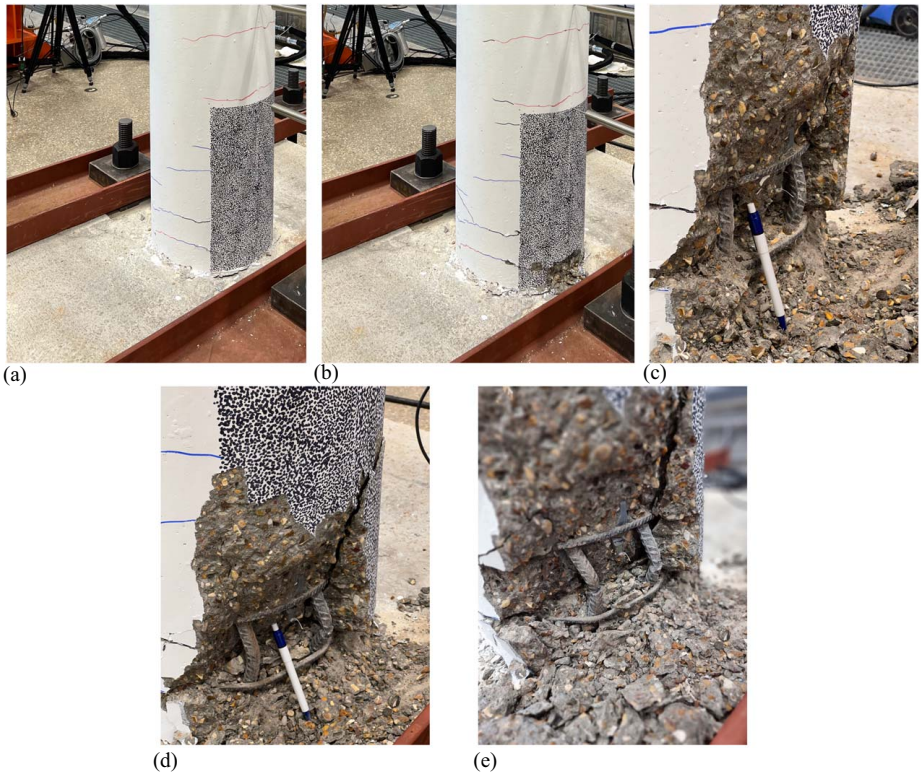

Fig. 11. Observed damage during the cyclic test of Column A: (a) bar slip at 2% drift; (b) cover concrete spalling at 3% drift; (c) visible bar buckling at 4% drift; (d) first bar fracture at 4.5% drift; and (e) second bar fracture during the last cycle at 4.5% drift.

and the curvature of the columns. The curvature [k_z (1/mm)] was evaluated using the following equation (Kashani et al. 2017):

$$k_z = \frac{(\varepsilon_2 - \varepsilon_1)}{d} \tag{1}$$

where ε_2 and ε_1 = vertical strains in the extreme tensile and compressive fibers of the column, respectively; and d = depth of the column (mm).

The moment–curvature relationships up to 1.33% drift (drift at ultimate strength of Column B1) for Columns A, A1, and B1 are compared and shown in Fig. 17. Column A demonstrated a lower cracking moment than the corroded columns in the negative

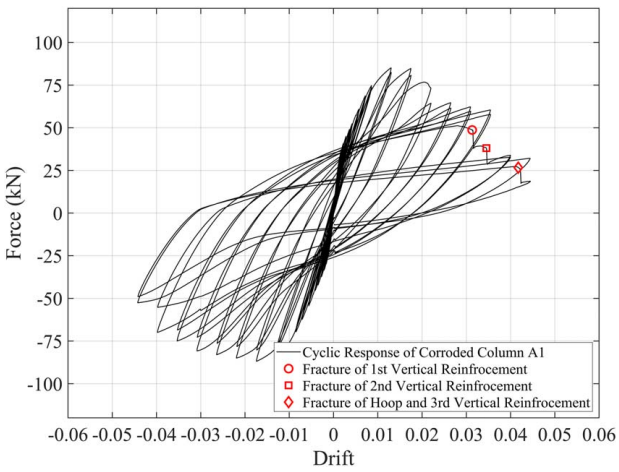

Fig. 12. Nonlinear cyclic response of corroded Column A1.

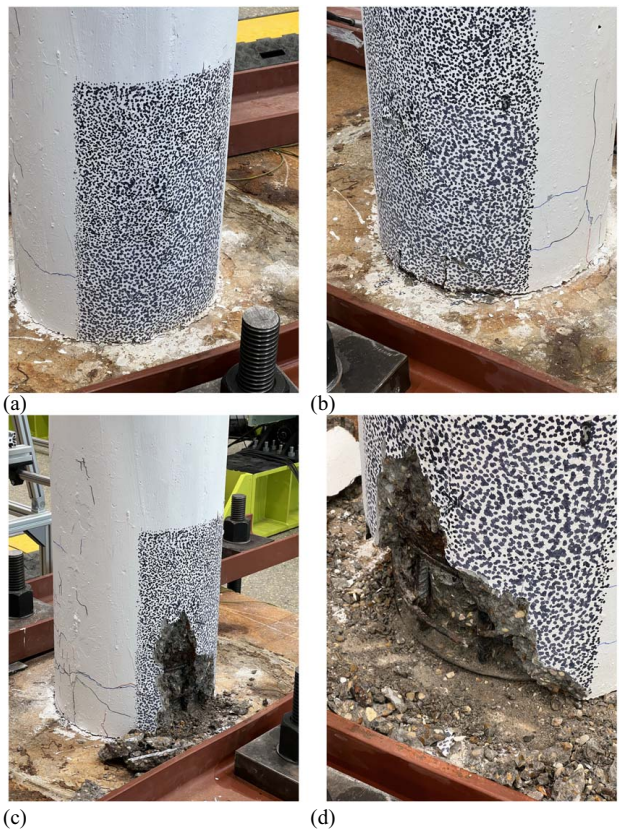

Fig. 13. Observed damage during the cyclic test of Column A1: (a) bar slip at 2% drift; (b) cover concrete spalling at 3% drift; (c) first and second bar fracture and significant concrete crushing at 3.5% drift; and (d) hoop fracture at 4% drift.

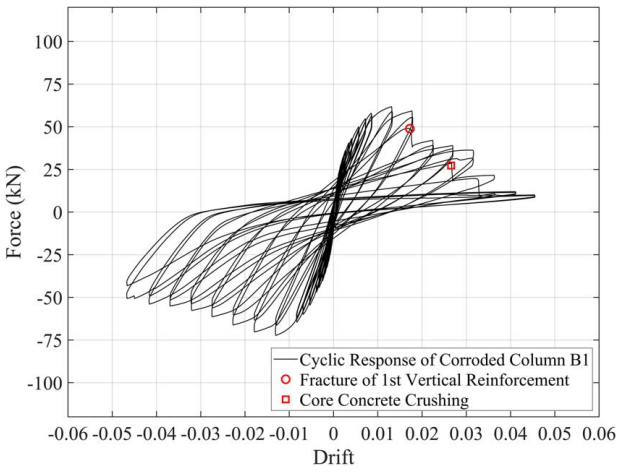

Fig. 14. Nonlinear cyclic response of corroded Column B1.

loading directions. This was partially due to the greater initial stiffness of the corroded columns and to construction tolerance. During the construction of Column A, some of the vertical bars were slightly displaced; therefore, the vertical bars were not equally spaced around the perimeter. This changed the cracking moment in Column A and different moment–curvature behavior in the positive–negative direction. The corroded columns demonstrated similar moment–curvature behavior in the positive loading direction up to 0.7×10^{-5} 1/mm, beyond which the moment of Column B1 almost plateaued. In addition, the moment of Column A surpassed that of the corroded columns at 0.7×10^{-5} 1/mm curvature in the positive loading direction. All columns reached similar curvature in the positive loading direction. In the negative loading direction, Column A reached a greater curvature than the corroded columns at 1% and 1.33% drifts. However, the moment of Column A was less than that of the corroded columns at the same curvature; Column A1 had a greater moment resistance than Column B1.

The neutral axis and axial strain on the longitudinal reinforcement were interpolated between the strain values in the extreme fibers of the columns. The neutral axis of Columns A1 and B1 initially advanced away from the center of the column and moved outward in the same direction as the loading direction. In contrast, Column A1's neutral axis at small drifts (< 0.3%) had a bias to the positive loading side; beyond these small drifts, the neutral axis then started to move outward in the same direction as the loading direction. Columns A, A1, and B1 demonstrated uneven neutral axis values when subjected to positive and negative loading, with a percentage difference in the neutral axis values in the positive and negative loading directions at 1% drift of 25.31%, 59.12%, and 104.56%, respectively. However, the percentage difference between neutral axis values in the positive and negative loading directions decreased in Columns A, A1, and B1 as the drift increased toward the ultimate load to 8.05%, 17.76, and 30.15%, respectively. The interpolated axial strain on the reinforcing bars showed that the first yield in the reinforcing bars occurred at 0.75%, 1%, and 0.6% drift for Columns A, A1, and B1, respectively.

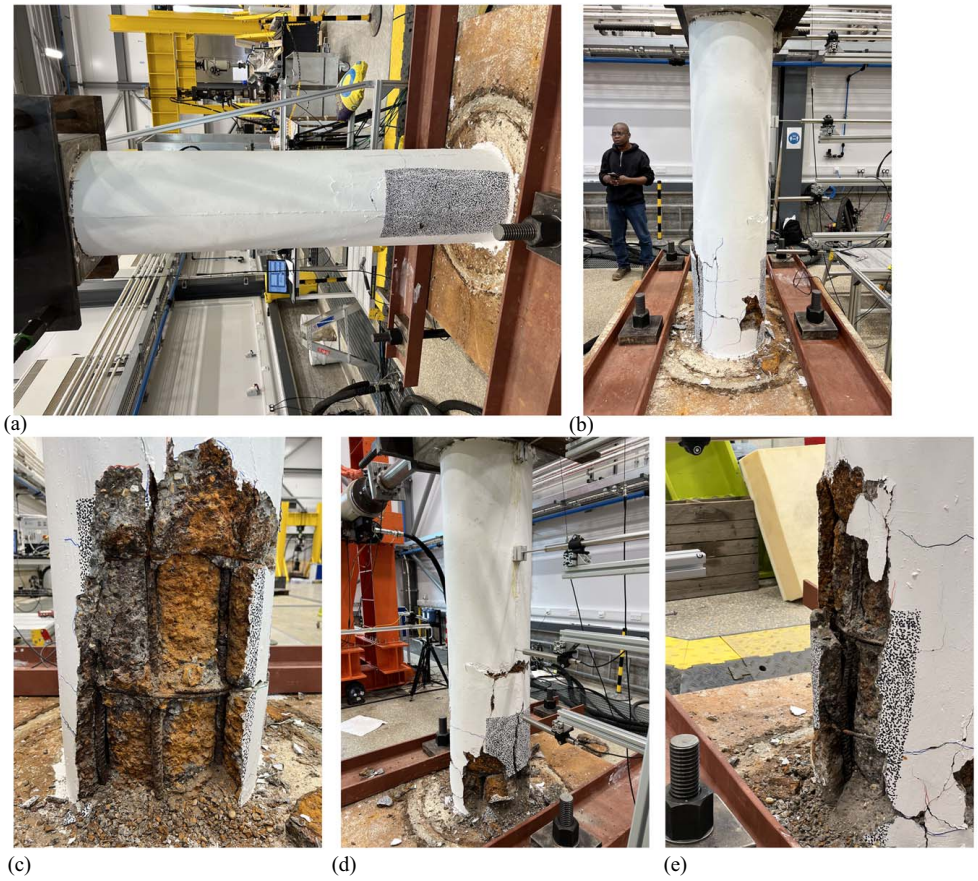

Fig. 15. Observed damage during the cyclic test of Column B1: (a) concrete cover crushing/spalling at 0.8% drift; (b) fracture of vertical bar and severe cover spalling at 2% drift; (c) visible buckling at 3% drift; (d) severe core concrete crushing at 3.5% drift; and (e) hoop fracture at 4% drift.

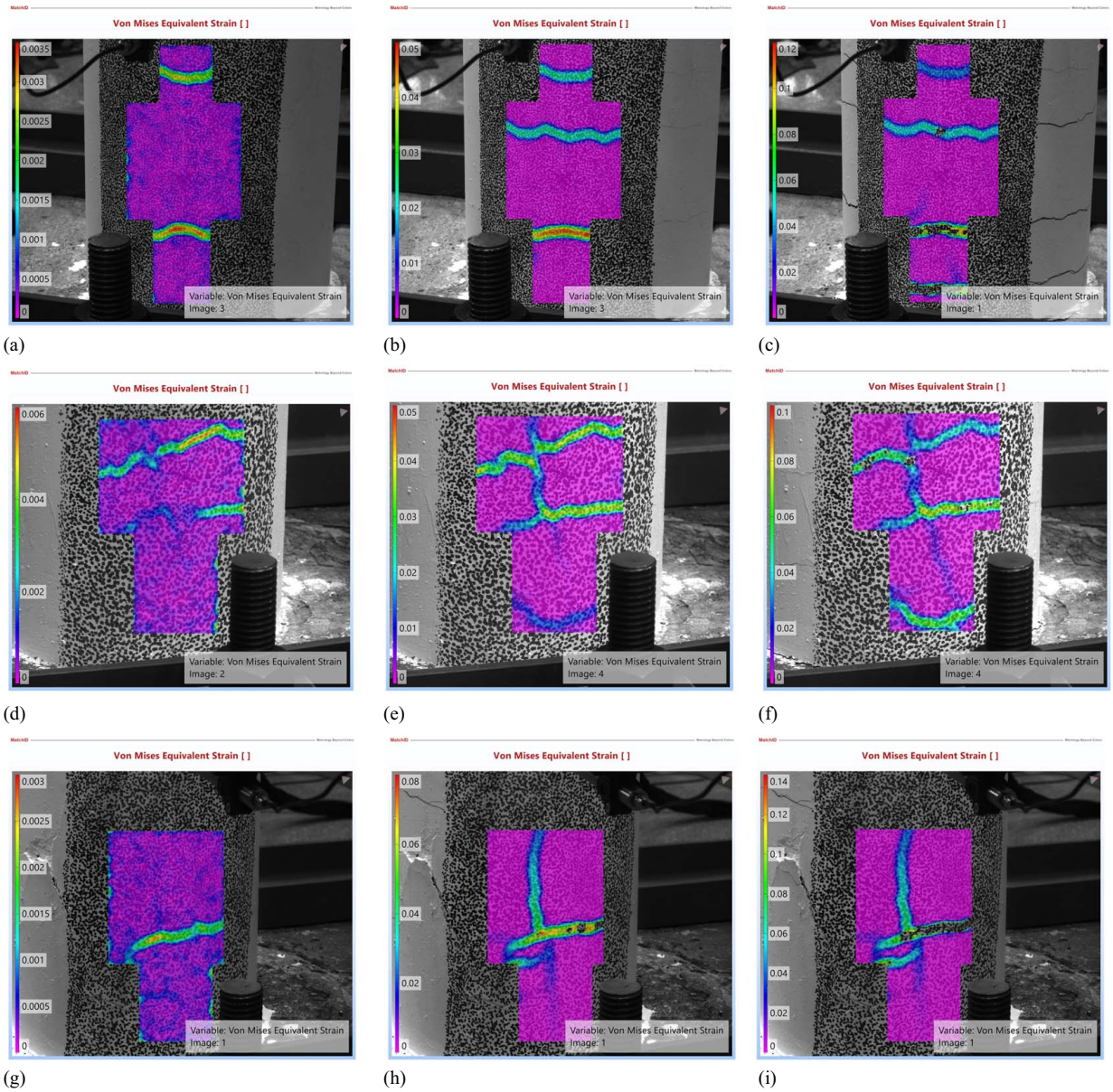

Fig. 16. DIC strain images at cracking moment, 1% drift and drift at ultimate strength of Columns: (a–c) A; (d–f) A1; and (g–i) B1.

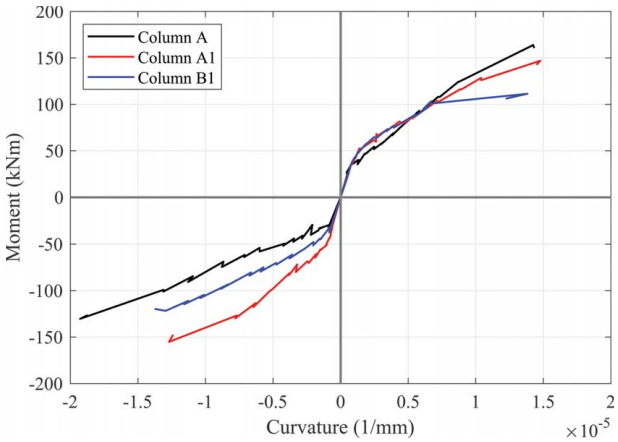

Fig. 17. Moment–curvature response of Columns A, A1, and B1 up to 1.33% drift.

For each cyclic loop, the mean flexural stiffness of the RC column was calculated from the moment–curvature relationships using

$$\mathrm{EI}_z = \frac{|M^+_{\max,i}| + |M^-_{\max,i}|}{|k^+_{z_{\max,i}}| + |k^-_{z_{\max,i}}|} \tag{2}$$

where EI_z = flexural stiffness of the column; $M_{\max,i}$ = peak moment in the positive and negative loading direction (kN.mm); and $k_{z\max,i}$ = peak curvature in the positive and negative direction for each loop (1/mm).

To compare the mean flexural stiffness from the moment–curvature to the secant stiffness, which represents the total stiffness (flexural, shear, and slip) from the force–displacement, the flexural and total stiffnesses for each column were normalized to their initial values. For Column A [Fig. 18(a)], the flexural stiffness degradation was greater than the total stiffness degradation, which might primarily be attributed to slipping in the reinforcing bar, because

J. Bridge Eng., 2024, 29(8): 04024048

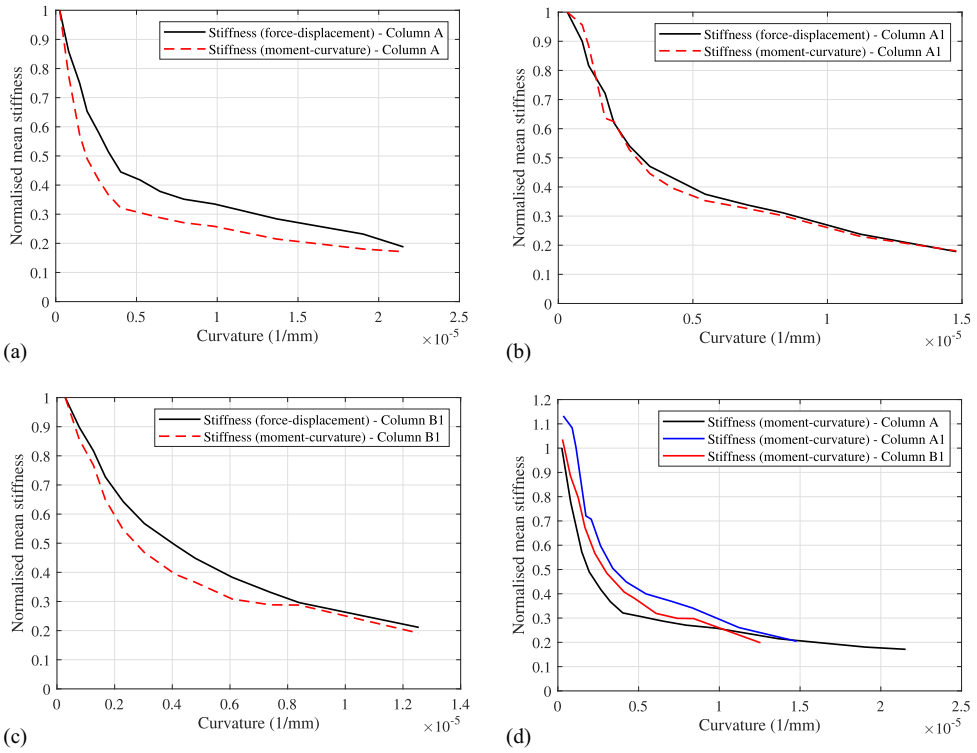

Fig. 18. Comparison of normalized mean stiffness from moment–curvature (DIC) and (a–c) force–displacement responses, and comparison of stiffness from moment–curvature between uncorroded; and (d) corroded columns.

shear is negligible in columns of moderate slenderness. However, beyond 5.0×10^{-6} 1/mm curvature, the flexural and total stiffness of Column A merged closer. In contrast to Column A, Column A1 showed that flexural stiffness and total stiffness were approximately identical up to 1.5×10^{-5} 1/mm curvature [Fig. 18(b)], which indicated that stiffness from the reinforcing bar slip was negligible in Column A1. Column B1 [Fig. 18(c)] initially demonstrated similar behavior to Column A up to 6×10^{-6} 1/mm curvature, after which flexural stiffness and total stiffness become approximately the same. In addition, the flexural stiffness degradation in all columns were compared and shown in Fig.18(d), the flexural stiffness values of all columns were normalized to the initial flexural stiffness value of uncorroded Column A. The initial flexural stiffness was greater, and initial stiffness degradation was lesser in the corroded columns than in uncorroded Column A. However, beyond 4.0×10^{-6} 1/mm curvature, the stiffness degradation of the corroded columns became greater than uncorroded Column A, with Columns B1 and A1 stiffness intersecting Column A's stiffness at curvatures of 1.0×10^{-5} and 1.4×10^{-5} 1/mm, respectively.

Impact of Corrosion on Effective Stiffness Degradation of RC Columns

The effective secant stiffness of the columns for each cyclic loop could be calculated using

$$K_{\text{sec}} = \frac{|F^{+}_{\text{max},i}| + |F^{-}_{\text{max},i}|}{|\delta^{+}_{\text{max},i}| + |\delta^{-}_{\text{max},i}|} \tag{3}$$

where K_{sec} = effective secant stiffness of the column (kN/m); $F_{\text{max},i}$ = peak force in positive and negative direction (kN); and $\delta_{\text{max},i}$ = is the peak displacement in positive and negative direction for each loop (m).

To compare the stiffness degradation of all the columns, the K_{sec} calculated for each loop in each column was normalized to the initial effective stiffness (K_{ses}) of uncorroded Column A. The normalized K_{sec} (Fig. 19) showed that the initial stiffness of the corroded columns was higher than the uncorroded columns until Cycle 11, which was less than a 0.5% drift ratio. However, as the drift ratio of the cyclic test increased, the stiffness degradation in the corroded columns became more significant than that of the corroded column. This was due to the more significant concrete damage in the corroded specimens under cyclic loading. In addition, the stiffness calculations confirmed that corrosion resulted in an increase in the initial stiffness of the columns, which was in good agreement with the impact hammer test results, which are shown in Fig. 9.

Impact of Corrosion Energy Dissipation Capacity

The hysteretic energy dissipation capacity is important when RC bridges are subjected to earthquake loading. Corrosion could significantly impact the energy dissipation capacity of aging bridges and, therefore, increase the seismic vulnerability of these bridges. The cumulative hysteretic energy dissipation of each column was calculated and normalized to the corresponding total dissipated energy during the cyclic tests, as shown in Figs. 20(a–c). The energy dissipation graphs for all columns show that there was almost no energy dissipation until Cycle 11, which was in good agreement with the stiffness degradation results shown in Fig. 19. To compare the energy dissipation capacity of the corroded and uncorroded columns, Fig. 20(d) shows the cumulative energy dissipation of all columns normalized to the total dissipated energy of the uncorroded column. Fig. 20(d) shows that corroded Column B1 has

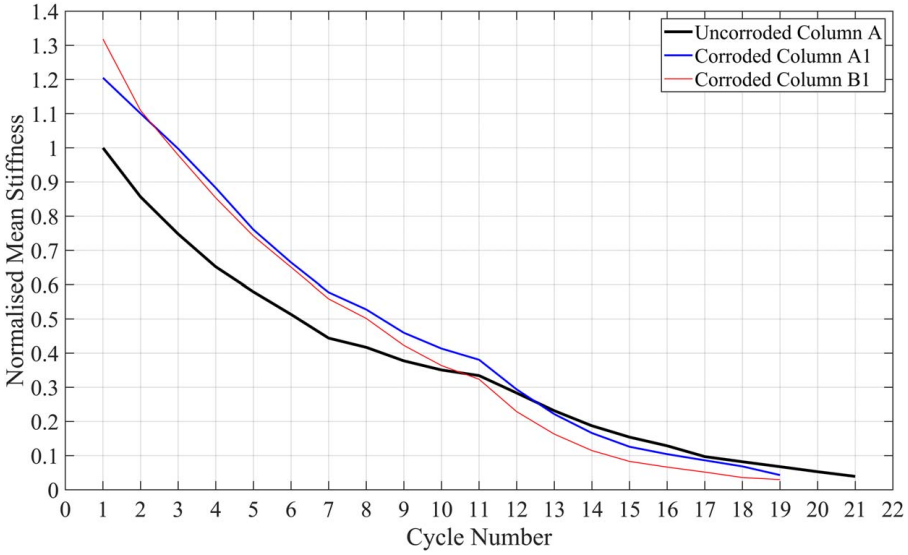

Fig. 19. Normalized effective stiffness of all columns.

the lowest energy dissipation capacity. This was due to higher average corrosion (compared with Column A1) and poor seismic detailing. Although Column A1 experienced fracture in three vertical bars due to localized corrosion at the base, the average corrosion in the same column was lower than corroded Column B1, where only one bar fractured in tension. However, corroded Column B1 experienced much more severe damage in the concrete, followed by buckling in the vertical bars due to the lack of confinement. This could be explained by comparing the nonlinear cyclic response and backbone curves for all three columns, as shown in Fig. 21. Fig. 21 shows that corrosion had a more significant impact on the ductility and energy dissipation capacity of RC columns than residual strength.

Impact of Corrosion on Equivalent Viscous Damping Ratio

The equivalent viscous damping ratio (ξ) represents the combined effects of elastic and hysteretic damping (Blandon and Priestley 2005). The modeling and calculation of the equivalent viscous damping ratio is available in Zhang et al. (2017) and is used here. Fig. 22 shows the calculated values of ξ for all three columns.

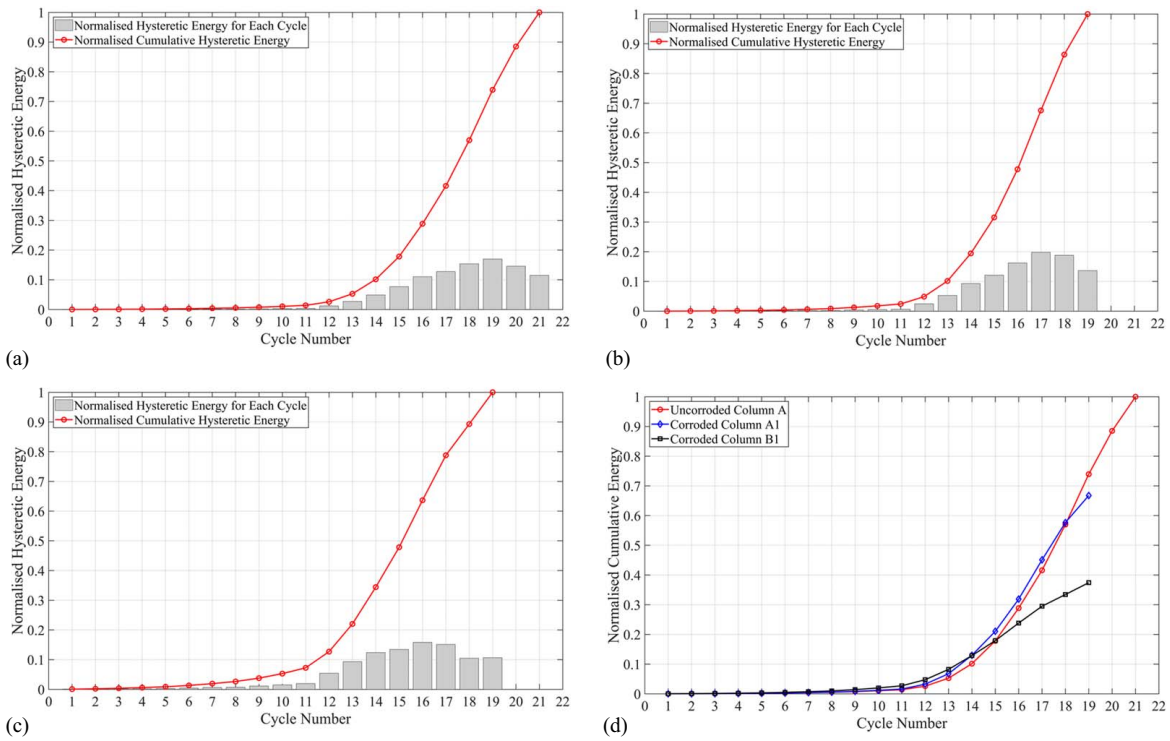

Fig. 20. Hysteretic energy dissipation: (a) uncorroded Column A; (b) corroded Column A1; (c) corroded Column B1; and (d) all columns.

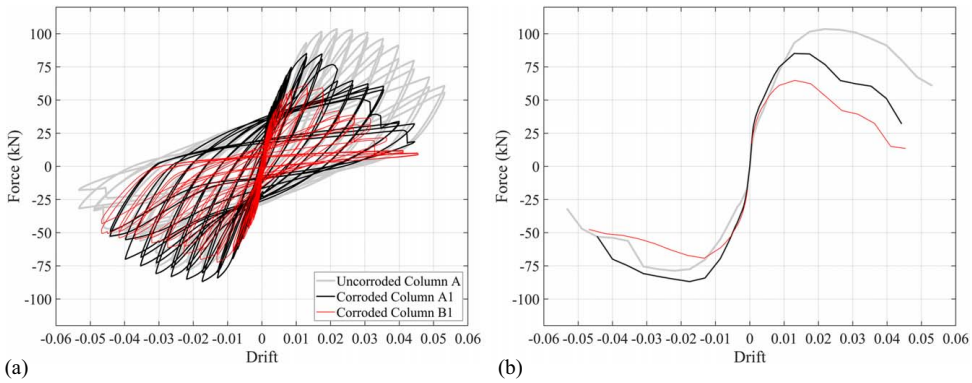

Fig. 21. Nonlinear response of all three columns: (a) cyclic response; and (b) backbone curves.

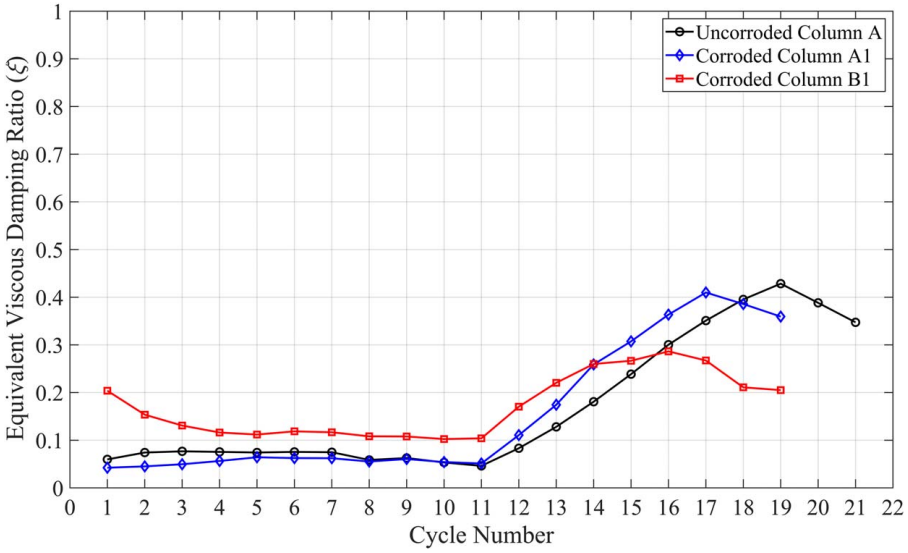

Fig. 22. Equivalent viscous damping ratio (ξ).

Similar to the energy dissipation capacity, ξ started increasing after Cycle11 and gradually decreased after severe damage. This showed that as the hysteretic energy increased, ξ increased, and after severe cyclic degradation, ξ decreased. Fig. 22 shows that ξ in corroded Column B1 was initially higher than in Columns A and A1, but the maximum ξ in corroded Column B1 was lower than the other two columns. This was due to the corrosion-induced severe damage in the concrete; therefore, the damage in the concrete resulted in more initial damping. However, as the drift ratio increased, the cyclic degradation resulted in a reduced damping ratio compared with Columns A and A1.

Conclusion

Three RC bridge piers with different reinforcement details and corrosion were tested under lateral cyclic loading. Column A was a well-confined uncorroded column, and Column A1 had the same RC detail with corrosion damage. Columns A and A1 were seismically detailed according to EC8. Column B1 was a lightly confined corroded column that represented aging bridge piers with non-code-conforming RC details. The main conclusions of this study can be summarized as follows.

1. The free vibration tests on the test specimens showed that the natural frequency of the columns increased after corrosion. This might be due to the increased internal pressure at the reinforcement and concrete interface, which increased the friction and bond.
2. Based on the previous conclusion, the cyclic tests showed that the initial effective stiffness of the corroded columns was more than that of the uncorroded specimen. However, when the drift ratio increased, the stiffness degradation in the corroded specimens was more significant than that of the uncorroded specimen.
3. The uncorroded column was seismically detailed according to EC8 criteria. However, significant inelastic buckling followed by low-cycle fatigue fracture of vertical bars was observed. This was due to the interaction between the hoop reinforcement and vertical bars, which is not explicitly captured in the current seismic design codes. This is an area for further research.
4. Nonuniform corrosion significantly impacted the failure mechanism of the corroded specimens. Corrosion in well-confined Column A1 was concentrated at the base of the column and, therefore, column failure was governed by localized fracture in the bars at the base of the column. Corrosion was more evenly distributed in Column B1, with some localized corrosion approximately 200 mm above the foundation. This resulted in significant damage to the concrete, followed by inelastic buckling and fracture in the vertical bars.

5. Corrosion had a more significant impact on the ductility and energy dissipation capacity loss than the strength loss in corroded columns. The test results showed that corrosion resulted in an approximate 5% loss of strength in Column A1 and a 20% loss of strength in Column B1. However, it resulted in an approximate 30% reduction in energy dissipation capacity in Column A1 and a 60% loss of energy dissipation capacity in Column B1.
6. The results showed that DIC data could be used to measure strain field and surface concrete damage at small drift ratios. However, the use of DIC could be challenging on curved surfaces. Therefore, multiple cameras are required for reliable data measurement.

Data Availability Statement

All data, models, or codes that support the findings of this study are available from the corresponding author upon reasonable request.

Acknowledgments

The authors thank Network Rail for their professional and financial support for this research. Furthermore, the authors acknowledge the support received by the UK Engineering and Physical Sciences Research Council for funding the experimental program under Grant No. EP/R039178/1. The experiments were conducted in the LSTL, which is part of the Collaboratorium for Research on Infrastructure and Cities National Infrastructure Laboratory, based at the University of Southampton. The help of Andrew Morgan, LSTL Technician, in setting-up the experiment is gratefully acknowledged.

Supplemental Materials

There are supplemental materials associated with this paper online in the ASCE Library (www.ascelibrary.org).

References

ACI (American Concrete Institute). 2013. *Guide for testing reinforced concrete structural elements under slowly applied simulated seismic loads*. ACI 374.2R-13. Farmington Hills, MI: ACI.

Al-Kamaki, Y. S. S. 2021. "Ultimate strain models derived using a Digital Image Correlation (DIC) system for preloaded RC columns subjected to heating and cooling and confined with CFRP sheets." *J. Build. Eng.* 41: 102306. https://doi.org/10.1016/j.jobe.2021.102306.

Aminulai, H. O., A. F. Robinson, N. S. Ferguson, and M. M. Kashani. 2023a. "Impact of corrosion on axial load capacity of ageing low-strength reinforced concrete columns with different confinement ratios." *Constr. Build. Mater.* 384: 131355. https://doi.org/10.1016/j.conbuildmat.2023.131355.

Aminulai, H. O., A. F. Robinson, N. S. Ferguson, and M. M. Kashani. 2023b. "Nonlinear behaviour of corrosion damaged low-strength short reinforced concrete columns under compressive axial cyclic loading." *Eng. Struct.* 289: 116245. https://doi.org/10.1016/j.engstruct.2023.116245.

Angst, U. M. 2018. "Challenges and opportunities in corrosion of steel in concrete." *Mater. Struct.* 51 (1): 1–20. https://doi.org/10.1617/s11527-017-1131-6.

Aquino, W., and N. M. Hawkins. 2007. "Seismic retrofitting of corroded reinforced concrete columns using carbon composites." *ACI Struct. J.* 104 (3): 348.

ASCE. 2021. *Report card for America's infrastructure*. New York: ASCE.

Barker, G., G. Beardsley, and A. Parsons. 2014. "The National Audit Office's value-for-money assessment of transport investments." Discussion Paper No. 2014-12 Prepared for the Roundtable: Ex-post Assessment of Transport Investments and Policy Interventions. London, UK: The National Audit Office.

Biondini, F., E. Camnasio, and A. Titi. 2015. "Seismic resilience of concrete structures under corrosion." *Earthquake Eng. Struct. Dyn.* 44 (14): 2445–2466. https://doi.org/10.1002/eqe.2591.

Blandon, C. A., and M. J. N. Priestley. 2005. "Equivalent viscous damping equations for direct displacement based design." *J. Earthquake Eng.* 9 (sup2): 257–278. https://doi.org/10.1142/S1363246905002390.

Broomfield, J. P. 2023. *Corrosion of steel in concrete: Understanding, investigation and repair*. Boca Raton, FL: CRC Press.

Camnasio, E. 2013. "Lifetime performance and seismic resilience of concrete structures exposed to corrosion." Ph.D thesis, Dept. of Civil and Environmental Engineering, Polytechnic University of Milan, Italy.

CEN (European Committee for Standardization). 2004. *Eurocode 2: Design of concrete structures—Part 2: Concrete bridges—design and detailing rules (BS EN 1992-2:2005)*. Brussels, Belgium: CEN.

CEN (European Committee for Standardization). 2005. *Eurocode 8: Design provisions of structures for earthquake resistance—Part 2: Bridges (EN1998-2: 2005)*. Brussels, Belgium: CEN.

Chan, K. S., and J. D. Cryer. 2008. *Time series analysis with applications in R*. 2nd ed. New York: Springer.

Dhakal, R. P., and K. Maekawa. 2002. "Reinforcement stability and fracture of cover concrete in reinforced concrete members." *J. Struct. Eng.* 128 (10): 1253–1262. https://doi.org/10.1061/(ASCE)0733-9445(2002)128:10(1253).

Di Carlo, F., A. Meda, and Z. Rinaldi. 2023. "Structural performance of corroded RC beams." *Eng. Struct.* 274: 115117. https://doi.org/10.1016/j.engstruct.2022.115117.

Dizaj, E. A., R. Madandoust, and M. M. Kashani. 2018a. "Probabilistic seismic vulnerability analysis of corroded reinforced concrete frames including spatial variability of pitting corrosion." *Soil Dyn. Earthquake Eng.* 114: 97–112. https://doi.org/10.1016/j.soildyn.2018.07.013.

Dizaj, E. A., R. Madandoust, and M. M. Kashani. 2018b. "Exploring the impact of chloride-induced corrosion on seismic damage limit states and residual capacity of reinforced concrete structures." *Struct. Infrastruct. Eng.* 14 (6): 714–729. https://doi.org/10.1080/15732479.2017.1359631.

Dizaj, E. A., M. R. Salami, and M. M. Kashani. 2023. "Seismic vulnerability analysis of irregular multi-span concrete bridges with different corrosion damage scenarios." *Soil Dyn. Earthquake Eng.* 165: 107678. https://doi.org/10.1016/j.soildyn.2022.107678.

Du, Y. G., L. A. Clark, and A. H. C. Chan. 2005a. "Residual capacity of corroded reinforcing bars." *Mag. Conc. Res.* 57 (3): 135–147. https://doi.org/10.1680/macr.2005.57.3.135.

Du, Y. G., L. A. Clark, and A. H. C. Chan. 2005b. "Effect of corrosion on ductility of reinforcing bars." *Mag. Conc Res* 57 (7): 407–419. https://doi.org/10.1680/macr.2005.57.7.407.

El Maaddawy, T. A., and K. A. Soudki. 2003. "Effectiveness of impressed current technique to simulate corrosion of steel reinforcement in concrete." *J. Mater. Civ. Eng.* 15 (1): 41–47. https://doi.org/10.1061/(ASCE)0899-1561(2003)15:1(41).

GCM, Gaal. 2004. "Prediction of deterioration of concrete." Ph.D. thesis, Dept. of Civil Engineering and Geosciences, University of Delft.

Ge, X., M. S. Dietz, N. A. Alexander, and M. M. Kashani. 2020. "Nonlinear dynamic behaviour of severely corroded reinforced concrete columns: Shaking table study." *Bull. Earthquake Eng.* 18 (4): 1417–1443. https://doi.org/10.1007/s10518-019-00749-3.

Ghosh, J., and J. E. Padgett. 2010. "Aging considerations in the development of time-dependent seismic fragility curves." *J. Struct. Eng.* 136 (12): 1497–1511. https://doi.org/10.1061/(ASCE)ST.1943-541X.0000260.

Imperatore, S., Z. Rinaldi, and C. Drago. 2017. "Degradation relationships for the mechanical properties of corroded steel rebars." *Constr. Build. Mater.* 148: 219–230. https://doi.org/10.1016/j.conbuildmat.2017.04.209.

Kashani, M. M. 2017. "Size effect on inelastic buckling behavior of accelerated pitted corroded bars in porous media." *J. Mater. Civ. Eng.* 29 (7): 04017022. https://doi.org/10.1061/(ASCE)MT.1943-5533.0001853.

Kashani, M. M., P. Alagheband, R. Khan, and S. Davis. 2015a. "Impact of corrosion on low-cycle fatigue degradation of reinforcing bars with the effect of inelastic buckling." *Int. J. Fatigue* 77: 174–185. https://doi.org/10.1016/j.ijfatigue.2015.03.013.

Kashani, M. M., A. J. Crewe, and N. A. Alexander. 2013. "Nonlinear cyclic response of corrosion-damaged reinforcing bars with the effect of buckling." *Constr. Build. Mater.* 41: 388–400. https://doi.org/10.1016/j.conbuildmat.2012.12.011.

Kashani, M. M., A. J. Crewe, and N. A. Alexander. 2017. "Structural capacity assessment of corroded RC bridge piers." *Proc. Inst. Civ. Eng.: Bridge Eng.* 170 (1): 28–41. https://doi.org/10.1680/jbren.15.00023.

Kashani, M. M., L. N. Lowes, A. J. Crewe, and N. A. Alexander. 2015b. "Phenomenological hysteretic model for corroded reinforcing bars including inelastic buckling and low-cycle fatigue degradation." *Comput. Struct.* 156: 58–71. https://doi.org/10.1016/j.compstruc.2015.04.005.

Kashani, M. M., J. Maddocks, and E. A. Dizaj. 2019. "Residual capacity of corroded reinforced concrete bridge components: State-of-the-art review." *J. Bridge Eng.* 24 (7): 03119001. https://doi.org/10.1061/(ASCE)BE.1943-5592.0001429.

Lee, H.-S., and Y.-S. Cho. 2009. "Evaluation of the mechanical properties of steel reinforcement embedded in concrete specimen as a function of the degree of reinforcement corrosion." *Int. J. Fract.* 157 (1–2): 81–88. https://doi.org/10.1007/s10704-009-9334-7.

Lee, H.-S., T. Kage, T. Noguchi, and F. Tomosawa. 2003. "An experimental study on the retrofitting effects of reinforced concrete columns damaged by rebar corrosion strengthened with carbon fiber sheets." *Cem. Concr. Res.* 33 (4): 563–570. https://doi.org/10.1016/S0008-8846(02)01004-9.

Li, C., H. Hao, H. Li, and K. Bi. 2015. "Seismic fragility analysis of reinforced concrete bridges with chloride induced corrosion subjected to spatially varying ground motions." *Int. J. Struct. Stab. Dyn.* 6: 1–27.

Liu, G., J. Cong, P. Wang, S. Du, L. Wang, and R. Chen. 2022. "Study on vertical vibration and transmission characteristics of railway ballast using impact hammer test." *Constr. Build. Mater.* 316: 125898. https://doi.org/10.1016/j.conbuildmat.2021.125898.

Liu, X., H. Jiang, and L. He. 2017. "Experimental investigation on seismic performance of corroded reinforced concrete moment-resisting frames." *Eng. Struct.* 153: 639–652. https://doi.org/10.1016/j.engstruct.2017.10.034.

Ma, Y., Y. Che, and J. Gong. 2012. "Behavior of corrosion damaged circular reinforced concrete columns under cyclic loading." *Constr. Build. Mater.* 29: 548–556. https://doi.org/10.1016/j.conbuildmat.2011.11.002.

Meda, A., S. Mostosi, Z. Rinaldi, and P. Riva. 2014. "Experimental evaluation of the corrosion influence on the cyclic behaviour of RC columns." *Eng. Struct.* 76: 112–123. https://doi.org/10.1016/j.engstruct.2014.06.043.

Otieno, M., G. Golden, M. G. Alexander, and H. Beushausen. 2019. "Acceleration of steel corrosion in concrete by cyclic wetting and drying: Effect of drying duration and concrete quality." *Mater. Struct.* 52 (2): 1–14. https://doi.org/10.1617/s11527-019-1349-6.

Rajput, A. S., and U. K. Sharma. 2018. "Corroded reinforced concrete columns under simulated seismic loading." *Eng. Struct.* 171: 453–463. https://doi.org/10.1016/j.engstruct.2018.05.097.

Rao, A. S., M. D. Lepech, and A. Kiremidjian. 2017. "Development of time-dependent fragility functions for deteriorating reinforced concrete bridge piers." *Struct. Infrastruct. Eng.* 13 (1): 67–83. https://doi.org/10.1080/15732479.2016.1198401.

Rinaldi, Z., F. Di Carlo, S. Spagnuolo, and A. Meda. 2022. "Influence of localised corrosion on the cyclic response of reinforced concrete columns." *Eng. Struct.* 256: 114037. https://doi.org/10.1016/j.engstruct.2022.114037.

Sun, Z., Y. Zheng, Y. Sun, X. Shao, and G. Wu. 2023. "Deformation ability of precast concrete columns reinforced with steel-FRP composite bars (SFCBs) based on the DIC method." *J. Build. Eng.* 68: 106083. https://doi.org/10.1016/j.jobe.2023.106083.

Verboven, P., P. Guillaume, B. Cauberghe, S. Vanlanduit, and E. Parloo. 2005. "A comparison of frequency-domain transfer function model estimator formulations for structural dynamics modelling." *J. Sound Vib.* 279 (3–5): 775–798. https://doi.org/10.1016/j.jsv.2003.11.046.

Yang, S.-Y., X.-B. Song, H.-X. Jia, X. Chen, and X.-L. Liu. 2016. "Experimental research on hysteretic behaviors of corroded reinforced concrete columns with different maximum amounts of corrosion of rebar." *Constr. Build. Mater.* 121: 319–327. https://doi.org/10.1016/j.conbuildmat.2016.06.002.

Yuan, W., A. Guo, and H. Li. 2017. "Experimental investigation on the cyclic behaviors of corroded coastal bridge piers with transfer of plastic hinge due to non-uniform corrosion." *Soil Dyn. Earthquake Eng.* 102: 112–123. https://doi.org/10.1016/j.soildyn.2017.08.019.

Zhang, Y.-Q., J.-X. Gong, Q. Zhang, and S. Han. 2017. "Equivalent damping ratio model of flexure-shear critical RC columns." *Eng. Struct.* 130: 52–66. https://doi.org/10.1016/j.engstruct.2016.10.003.